ISSN 1063-7842, Technical Physics, 2015, Vol. 60, No. 9, pp. 1348–1352. © Pleiades Publishing, Ltd., 2015.
Original Russian Text © F.F. Komarov, G.A. Ismailova, O.V. Mil'chanin, I.N. Parkhomenko, F.B. Zhusipbekova, G.Sh. Yar-Mukhamedova, 2015, published in Zhurnal Tekhnicheskoi Fiziki, 2015, Vol. 85, No. 9, pp. 91–96.

SOLID STATE ELECTRONICS

Effect of Thermal Processing on the Structure and Optical Properties of Crystalline Silicon with GaSb Nanocrystals Formed with the Aid of High-Doze Ion Implantation

F. F. Komarov[a], G. A. Ismailova[b]*, O. V. Mil'chanin[a], I. N. Parkhomenko[a], F. B. Zhusipbekova[b], and G. Sh. Yar-Mukhamedova[b]**

[a] *Belarus State University, pr. Nezavisimosti 4, Minsk, 220030 Belarus*
[b] *Al-Farabi National University, pr. Al-Farabi 71, Almaty, 050038 Kazakhstan*
**e-mail: gusel_a81@mail.ru*
***e-mail: Zh.fariza@mail.ru*

Received October 24, 2014; in final form, February 26, 2015

Abstract—Rutherford backscattering and transmission electron microscopy (TEM) are used to study distributions of impurities and structure of the GaSb + Si nanocomposites in several regimes of ion implantation and thermal processing. It is demonstrated that the hot implantation and annealing lead to a significant loss of impurity and the shift of the maximum concentration of impurity atoms toward the surface. The TEM data prove the formation of nanocrystals with sizes ranging from 20 to 100 nm, dislocation defects, and residual mechanical stresses. Raman spectroscopy is used to study the structure and phase composition of experimental silicon samples containing various nanocrystalline impurities.

DOI: 10.1134/S1063784215090078

INTRODUCTION

There has been considerable recent interest in the methods for improvement of light-emitting properties of silicon crystals that serve as the base material for micro- and nanoelectronics. A promising method for an increase in the optical yield of silicon employs specific features of nanosized particles in silicon and silicon dioxide and the influence of the quantum-dimensional effect on the intensity and spectral position of the emission bands [1, 2]. An important approach to the integration of optically efficient A^3B^5 materials and silicon involves the formation of quantum dots of the A^3B^5 semiconductors in crystalline silicon and silicon dioxide [2–4]. The creation of light-emitting structures of the IR and visible spectral ranges will make it possible to use relatively fast optical commutation rather than electron transfer in extra- and ultra-large scale ICs and, hence, increase the working rate and decrease the sizes of electronic elements. The purpose of this work is the formation of the GaSb nanocrystals in silicon with the aid of high-fluence ion implantation and thermal processing and the study of the structural and optical properties of such a nanocomposite system.

EXPERIMENTAL PROCEDURES

The nanocomposite structures are fabricated using the ion implantation of the antimony and gallium atoms and the subsequent thermal processing. The high-doze ion implantation leads to the formation of oversaturated solution of the impurity in the near-surface layer of the matrix. The post-implantation annealing causes the precipitation of impurity in nanoclusters (nanocrystals). For the creation of the composite layers on silicon that emit in the near-IR spectral range, we perform sequential implantation of the Sb^+ ions ($E = 350$ keV) and Ga^+ ions ($E = 250$ keV) at a fluence of 3.5×10^6 ions/cm^2 in both cases. The Sb^+ and Ga^+ ions are implanted at a temperature of $T = 500$°C to avoid amorphization of the silicon matrix in the course of irradiation. The computer simulation of the distributions of impurity atoms with respect to the depth in a silicon crystal is performed with the aid of the SRIM-2000 software (Stopping and Range of Ions in Matter) to preliminary choose the optimal energy and fluence of ions. Such an approach makes it possible to reach totally overlapped concentration profiles of impurities and obtain oversaturation at a level of 10 at %.

The thermal processing is performed in inert medium (argon) in the JET-FIRST-100 system for equilibrium and fast thermal processing. The structure of the resulting layers is studied using the small-angle X-ray diffraction and transmission electron microscopy (TEM) with the aid of a Hitachi H-800 200-keV electron microscope. The samples for the TEM experiments are transparent for the electron beam with an energy of 200 keV (the thickness is no greater than 150–200 nm). The impurity distribution over the

depth in the target is measured using Rutherford backscattering (RBS) of the He^+ ions with an energy of 1.5 MeV.

The optical properties of the samples are studied with the aid of Raman scattering. The Raman spectra are measured using a RAMANOR U-100 setup with a dispersion spectrometer. The laser excitation wavelength is $\lambda = 532$ nm, and the scattered radiation is collected in the backscattering configuration. The spectra are measured in a spectral interval of 90–600 cm^{-1} at room temperature.

RESULTS AND DISCUSSION

Figure 1 presents the concentration profiles of the Sb and Ga ions in the silicon matrix that are calculated using the SRIM software and obtained from the RBS spectra. The SRIM calculations do not take into account the temperature of the irradiated target and can be used to describe the processes of ion implantation at room or lower temperature. Figure 1 shows that the ion implantation at a temperature of 500°C causes significant broadening of the concentration profiles and a noticeable decrease in the concentration of impurity in comparison with the result of the SRIM calculations. This can be due to the effect of nonequilibrium accelerated diffusion. The equilibrium diffusion of the Sb and Ga atoms is observed in Si only at a temperature of $T = 900$°C [5]. Figure 1b shows the RBS spectra of the silicon samples implanted with Sb and Ga. Note that the high-temperature annealing leads to a further redistribution of impurity.

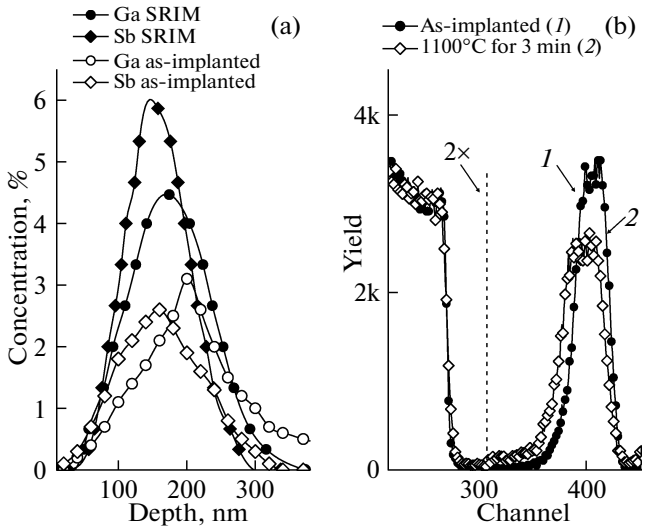

Fig. 1. (a) Results of the SRIM simulation and experimental profiles of the impurity concentrations in silicon upon implantation with the Ga (250 keV, 3.5×10^{16} cm^{-2}) and Sb (350 keV, 3.5×10^{16} cm^{-2}) ions and (b) backscattering spectrum of the silicon sample implanted with the Sb and Ga ions after 3-min-long thermal processing at a temperature of $T = 1100$°C.

Figure 2 illustrates the structure of silicon implanted with Sb and Ga and thermally processed. Even the hot implantation and thermal processing at a temperature of 900°C under conditions for the high-fluence implantation of the heavy (Sb and Ga) ions does not allow complete elimination of the defects of the Si crystalline lattice. The 45-min-long post-implantation annealing at a temperature of 900°C does not lead to acceptable reconstruction of the structure. The near-surface region of the Si sample contains a substantially damaged layer with precipitates and microtwins. The sizes of most precipitates range from 10 to 50 nm, and, for a small part of clusters, the sizes are 70–100 nm. The crystalline structure of precipitates is proven for several nanoprecipitates by the presence of the Moire patterns obtained at high resolution.

Note the presence of small extrareflexes near the basic reflexes of silicon on the diffraction pattern (Fig. 2a). The positions of such reflexes correspond to the reflexes of the Si microtwins. Figure 2a shows the dark-field image that is recorded for the ⟨200⟩-reflex of silicon. The extrareflexes are supplemented with the glow of the nanocluster–Si interfaces (arrows in Fig. 2c). Such an effect was observed in [4] for Si with the InAs nanoclusters. We assume that the reason lies in the relaxation of stresses at the interface of the A^3B^5 nanocrystal and Si due to the formation of fine dislocation networks. The mechanical stresses result from a significant mismatch of the parameters of the Si-matrix lattice and the lattice of the A^3B^5 nanocrystals. For the GaSb nanocrystals, the mismatch of the lattice constants is 12.2%.

Several samples are thermally processed at a temperature of $T = 1100$°C over 1 h for better reconstruction of the structure. Figures 3a, 3b, and 3d show the TEM images of such samples. It is seen that an increase in the temperature leads to substantial reconstruction of the structure of the damaged layer in comparison with the thermal processing at 900°C. The sizes of most precipitates range from 20 to 90 nm. However, several precipitates have sizes of up to 120 nm (Fig. 3c). The crystalline nature of the precipitates is proven by the Moire contrast on the images of clusters that are obtained at higher resolution (not shown). We also observe dislocation lines that connect the largest precipitates (arrows in Figs. 3b and 3d). Small dislocations are concentrated in the vicinity of nanoclusters on the high-resolution images. The glow of the nanocluster–Si interfaces is also observed on the dark-field image (as in the case of the 45-min-long annealing at a temperature of 900°C). We may assume that such an effect in the interface regions of the GaSb nanocrystals is caused by the radiative recombination of carriers (electrons and holes) that are generated by the incident electron beam (cathode luminescence). Small dislocations that are located in the vicinity of nanocrystals and dislocation lines that connect small precipitates may serve as the centers of the radiative

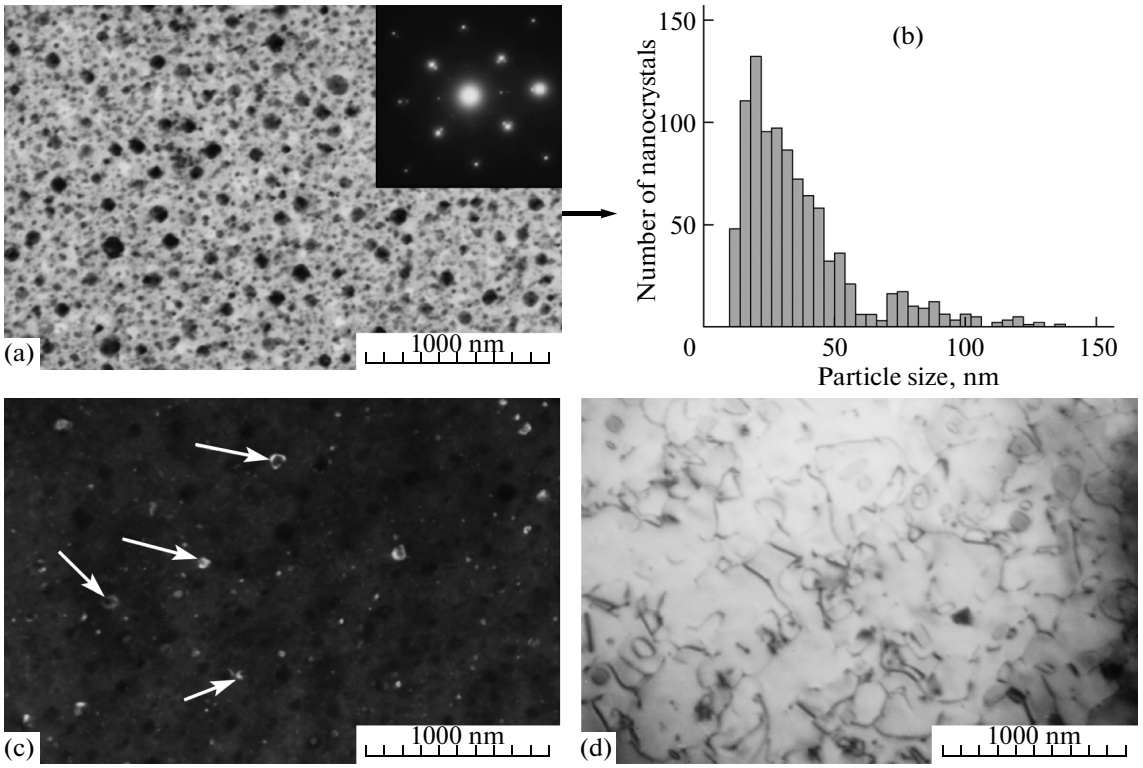

Fig. 2. (a, d) Light- and (c) dark-field TEM images and (b) size distribution of precipitates for the silicon samples after hot implantation of the Sb (350 keV, 3.5×10^{16} cm^{-2}) and Ga (250 keV, 3.5×10^{16} cm^{-2}) ions and 45-min-long annealing at a temperature of 900°C.

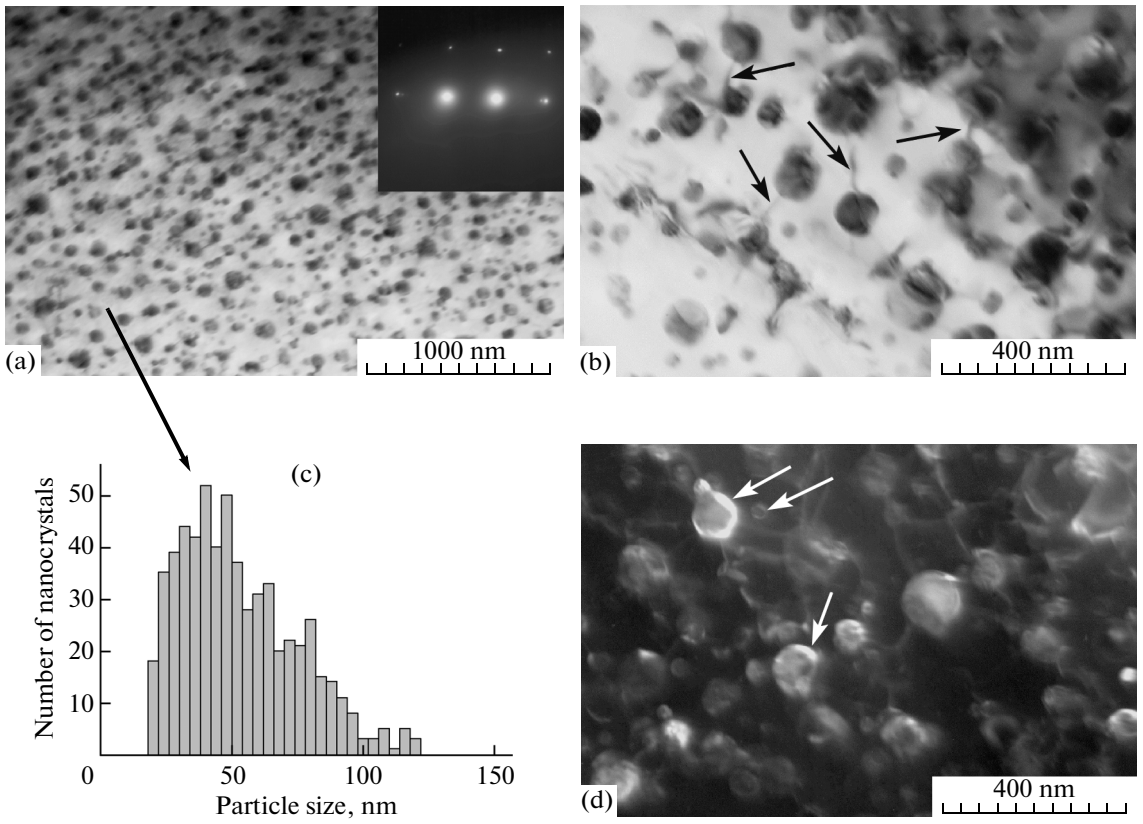

Fig. 3. (a, b) Light- and (d) dark-field TEM images and (c) size distribution of precipitates for the silicon samples after hot implantations of the Sb and Ga ions and 60-min-long annealing at a temperature of 1100°C.

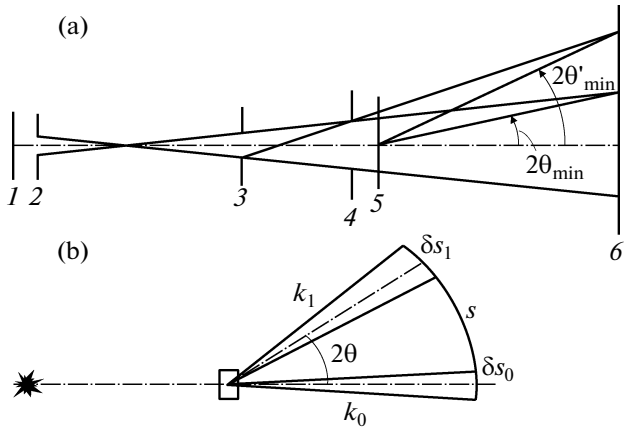

Fig. 4. Schemes that illustrate the formation of primary and scattered radiation at small scattering angles in (a) forward and (b) backward spaces: (*1*) radiation source, (*2–4*) circular apertures of collimator, (*5*) sample, and (*6*) detector plane.

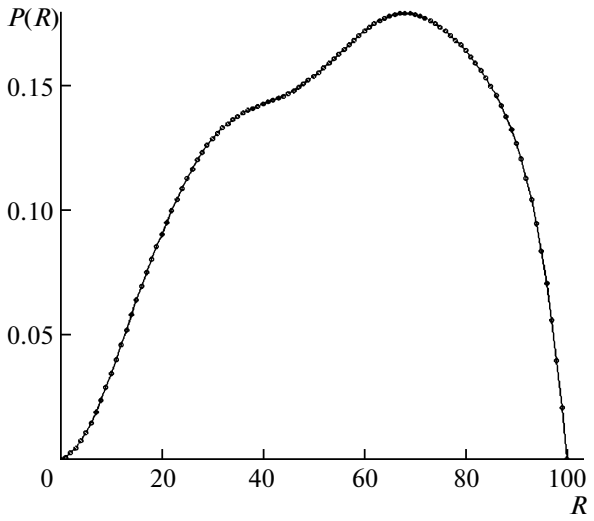

Fig. 5. Correlation function of the single-crystalline Si sample implanted with the Ga^+ (250 keV, 3.5×10^{16} cm^{-2}) and Sb^+ (350 keV, 3.5×10^{16} cm^{-2}) ions after 1-h-long thermal processing at a temperature of $T = 1100$°C.

recombination of carriers. The room-temperature dislocation luminescence of the ion-implanted silicon is actively studied for the construction of efficient silicon LEDs [6–9].

To identify the size distribution of the nanoprecipitates, we employ the small-angle X-ray diffractometry. The small-angle X-ray scattering (SAXS) is based on the measurement of the scattered intensity at different diffraction angles. The analysis of the SAXS data makes it possible to determine the parameters of dimensional effects from interfaces of the regions with different electron densities (from nanoparticles and/or pores): shape, sizes, and dispersion composition. The structure of a particle can be characterized with the aid of the correlation function that is directly calculated using the SAXS data:

$$\gamma(r) = (1/2\pi^2)\int I(h)(\sin hrh^2/hr)\partial h. \qquad (1)$$

Here, $\gamma(r)$ is the correlation function (averaged self-convolution of density) of particle that was introduced by Debye and Buche in the problems of small-angle scattering, $I(h)$ is the intensity of the small-angle scattering, and h and r are the elements of solid angle. The given expressions for $I(h)$ and $\gamma(r)$ are important for the analysis of the small-angle data. In particular, it is seen that $\gamma(r) = 0$ at $r > D$, where D is the maximum size of the particle. Function $\gamma(r)$ and function $P(r) = r^2\gamma(r)$ (distribution function with respect to distances) are widely employed in the problems of small-angle scattering. The functions are related to both configuration of particle (quantitatively describe a set of segments that connect the elements of the particle volume) and the distribution of inhomogeneities in the particle. The SAXS data are obtained using small-angle X-ray diffractometers.

A collimator of the primary monochromatic beam is used to form a narrow X-ray beam that is incident on the sample (Fig. 4). A system of small-size circular apertures that are located at relatively large (in comparison with aperture size) distances from each other makes it possible to form a wave that is close to the plane wave accurate to a ratio of r/R, where r and R are the diameters of apertures and distances between them, respectively. Ratio r/R determines the size of the projection of the primary beam in the detector plane. The ratio and sample–detector distance L are used to determine minimum angle $2\theta_{min}$ (and parameter h_{min}) above which we can measure the scattered intensity. Parameter h_{min} determines the small-angle resolution of the above collimation scheme and the upper-bound limit (D_{max}) of the size of inhomogeneities that can be studied using the diffractometer: $D_{max} = \pi/h_{min}$.

The SAXS data are used to obtain the correlation function for the implanted layers of nanocomposites (Fig. 5). The curve of the correlation function exhibits reflexes that are responsible for the spread of particle sizes. The curve position corresponds to spherical particles. The size distribution function (Fig. 6) indicates that most particles have sizes ranging from 20 to 100 nm, which is in good agreement with the TEM results (Fig. 3).

The Raman spectrum of the Si samples implanted with the Ga^+ and Sb^+ ions and annealed in different regimes contains the LO band that is responsible for light scattering by the GaSb crystalline precipitates (Fig. 7). This circumstance proves the crystalline structure of nanoprecipitates that is revealed in the TEM study. High-rate diffusion of the antimony atoms toward the Si surface leads to the formation of

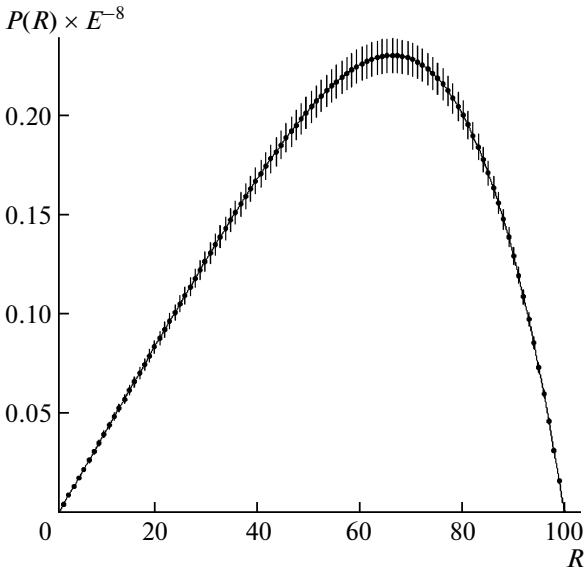

Fig. 6. Size distribution function for particles of the single-crystalline Si sample implanted with the Ga^+ (250 keV, 3.5×10^{16} cm^{-2}) and Sb^+ (350 keV, 3.5×10^{16} cm^{-2}) ions after 1-h-long thermal processing at a temperature of $T =$ 1100°C.

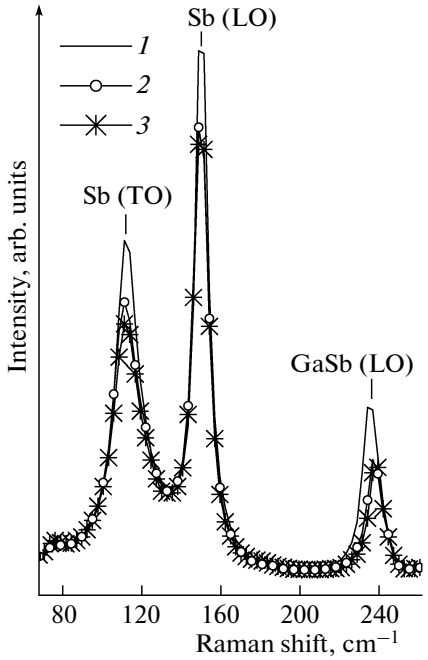

Fig. 7. Raman spectra of the silicon samples implanted with the Sb and Ga ions and annealed at a temperature of 1100°C over (*1*) 3, (*2*) 30, and (*3*) 60 min.

the Sb nanocrystals (TO and LO bands in the Raman spectrum in Fig. 7).

CONCLUSIONS

The RBS data show that the hot implantation of ions leads to developed broadening of the concentration profiles due to the effect of the nonequilibrium radiation-stimulated diffusion of the impurity. The subsequent thermal processing causes further redistribution of impurities in the implanted layer and a decrease in the impurity concentration. The crystalline structure of the nanoprecipitates is proven by the presence of the Moire contrast on the high-resolution TEM images from clusters and the Raman spectra. The glow of the GaSb nanocrystal–Si interfaces is observed on the dark-field TEM images. Apparently, such a glow of interfaces is related to the radiative recombination of carriers that are generated by incident electrons. Small dislocations that are concentrated in the vicinity of the GaSb nanocrystals and the dislocation lines that connect small precipitates may serve as efficient centers of the radiative recombination.

The SAXS data show that the clusters have spherical shapes and the sizes of particles range from 20 to 100 nm. These results are in good agreement with the TEM data.

REFERENCES

1. Y. Arakawa and H. Sakaki, Appl. Phys. Lett. **40**, 939 (1982).
2. N. Gerasimenko and Yu. Parkhomen'ko, *World of Materials and Nanotechnologies. Silicon—Material of Nanoelectronics* (Tekhnosfera, Moscow, 2007).
3. F. Komarov, L. Vlasukova, W. Wesch, A. Kamarou, O. Milchanin, S. Grechnyi, A. Mudryi, and A. Ivaniukovich, Nucl. Instrum. Methods Phys. Res. B **266**, 3557 (2008).
4. F. Komarov, L. Vlasukova, O. Milchanin, W. Wesch, E. Wendler, and J. Zuk, Mater. Sci. Eng., B **178**, 1169 (2013).
5. F. F. Komarov and A. F. Komarov, *Physical Processes on Ion Implantation in Solids* (UP Tekhno-Print, Minsk, 2001).
6. N. A. Sobolev, A. M. Emel'yanov, V. V. Zabrodskaya, R. L. Sukhanov, and E. I. Sheek, Semiconductors **41**, 537 (2007).
7. N. A. Sobolev, A. M. Emel'yanov, V. I. Sakharov, I. T. Serenkov, E. I. Sheek, and D. I. Tetel'baum, Semiconductors **41**, 616 (2007).
8. M. Milosavljevič, M. A. Lourenco, G. Shao, R. M. Gwilliam, and K. P. Homewood, Nucl. Instrum. Methods Phys. Res. B **266**, 2470 (2008).
9. N. A. Sobolev, in *Proceedings of the 5th All-Russia Conference on Physicochemical Grounds of Ion Implantation, Nizhny Novgorod, 2014*, pp. 59–60.

Translated by A. Chikishev